

# 1 **Limitations of ozone data assimilation with adjustment of NO<sub>x</sub> emissions: mixed** 2 **effects on NO<sub>2</sub> forecast over Beijing and surrounding areas**

3 X. Tang<sup>1</sup>, J. Zhu<sup>1</sup>, Z.F. Wang<sup>1</sup>, A. Gbaguidi<sup>2</sup>, C.Y. Lin<sup>3</sup>, J.Y. Xin<sup>1</sup>, T. Song<sup>1</sup>, B. Hu<sup>1</sup>

4 <sup>1</sup>LAPC, Institute of Atmospheric Physics, Chinese Academy of Sciences, Beijing, China

5 <sup>2</sup>AECOM Asia, Hong Kong, China

6 <sup>3</sup>Aviation Meteorological Center, Air Traffic Management Bureau, Civil Aviation Administration of  
7 China, Beijing, China

8 Correspondence to: X. Tang (tangxiao@mail.iap.ac.cn)

## 9 **Abstract**

10 This study investigates a cross-variable ozone data assimilation (DA) method based on an ensemble  
11 Kalman filter (EnKF) that has been used in the companion study to improve ozone forecasts over  
12 Beijing and surrounding areas. The main purpose is to delve into the impacts of the cross-variable  
13 adjustment of nitrogen oxides (NO<sub>x</sub>) emissions on the nitrogen dioxide (NO<sub>2</sub>) forecasts over this  
14 region during the 2008 Beijing Olympic Games. A mixed effect on the NO<sub>2</sub> forecasts was observed  
15 through application of the cross-variable assimilation approach in the real-data assimilation (RDA)  
16 experiments. The method improved the NO<sub>2</sub> forecasts over almost half of the urban sites with  
17 reductions of the root mean square errors (RMSEs) by 15%~36% in contrast to big increases of the  
18 RMSEs over other urban stations by 56%~239%. Over the urban stations with negative DA impacts,  
19 improvement of the NO<sub>2</sub> forecasts (with 7% reduction of the RMSEs) was noticed in night and  
20 morning versus significant deterioration in daytime (with 190% increase of the RMSEs), suggesting  
21 that the negative DA impacts mainly occurred during daytime. Ideal data assimilation (IDA)  
22 experiments with a box model and the same cross-variable assimilation method confirmed the mixed  
23 effects found in the RDA experiments. In the same tendency, NO<sub>x</sub> emission estimation was  
24 improved in night and morning even under large biases in the prior emission, while deteriorated in  
25 daytime (except for the case of minor errors in the prior emission). The mixed effects observed in the  
26 cross-variable DA, i.e., positive DA impacts on NO<sub>2</sub> forecast over some urban sites, negative DA  
27 impacts over the other urban sites and weak DA impacts over suburban sites, highlighted the  
28 limitations of the EnKF under strong nonlinear relationships between chemical variables. Under  
29 strong nonlinearity between daytime ozone concentrations and NO<sub>x</sub> emissions uncertainties (with  
30 large biases in the a prior emission), the EnKF may come up with inefficient or wrong adjustment to  
31 NO<sub>x</sub> emissions. The present findings reveal that bias correction is essential for the application of the

1 EnKF in dealing with the DA inconsistency over strong nonlinear system.

## 2 **1. Introduction**

3 Chemical data assimilation (CDA) integrates models and observations to better represent the  
4 chemical state of the atmosphere and is recognized as a technique for improving the simulations and  
5 forecasts of air pollutants such as ozone and aerosols (Carmichael et al., 2008; Sandu et al., 2011;  
6 Zhang et al., 2012). The role of CDA in optimizing initial and boundary conditions has been explored  
7 in several applications to improve forecasts of ozone and aerosol (Gaubert et al., 2014; Pagowski et  
8 al., 2014). Nevertheless, significant challenges persist in CDA.

9 One of the major challenges in CDA is that the impact of the initial conditions on the forecast of  
10 air pollutants such as ozone decreases with simulation time (Gaubert et al., 2014; Jimenez et al.,  
11 2006). To overcome such obstacle, emissions with large uncertainties and strong impacts on air  
12 quality modeling, identified as the crucial sources of uncertainties and considered to be the key  
13 control variables (Beekmann and Derognat, 2003; Hanna et al., 2001), have been integrated into the  
14 CDA. The importance of emissions as control variables in the CDA has also been documented  
15 recently (Carmichael et al., 2008; Koohkan et al., 2013; Zhang et al., 2012). Accordingly, advanced  
16 CDA techniques that enable inverse or cross-variable adjustments of emissions have been established  
17 and their applications have provided significant improvement of ozone forecasts (e.g., Tang et al.,  
18 2011).

19 However, the performances of such advanced CDA on the forecasts of other pollutants related to  
20 ozone are rarely reported and have not aroused enough attention. In this field, few studies stand out  
21 (Elbern et al., 2007; van Loon et al., 2000). Elbern et al., (2007) carried out two sets of data  
22 assimilation experiments with a four dimensional variational inversion method: (1) assimilation of  
23 ozone ( $O_3$ ) and nitrogen dioxide ( $NO_2$ ) observations simultaneously, and (2) assimilation of only  $O_3$   
24 observations. Both experiments resulted in reductions of nitrogen oxides ( $NO_x$ ) emissions after data  
25 assimilation in most cases even if the model underestimated the  $NO_x$  concentrations before data  
26 assimilation. Similar results were reported by van Loon et al. (2000) through the assimilation of  $O_3$   
27 observations and adjustments of sulfur oxides ( $SO_x$ ) emissions using an ensemble Kalman filter. The  
28 method enhanced the emission rates of  $SO_x$  when significant over-prediction of  $SO_2$  concentrations  
29 subsisted. Such inconsistencies, i.e., the emissions enhanced under the overestimation of

1 concentrations or the emissions reduced under the underestimation of concentrations, reveal some  
2 gaps between ozone forecast improvement and precursor emission optimization and call for a  
3 comprehensive evaluation of the cross-variable chemical data assimilation techniques.

4 Tang et al. (2011) employed a high horizontal resolution (9km) model to perform the  
5 assimilation of O<sub>3</sub> observations with the ensemble Kalman filter and the adjustment of NO<sub>x</sub>  
6 emissions for O<sub>3</sub> forecast improvement over Beijing and its surrounding areas. However, the impact  
7 of ozone assimilation on the precursor (NO<sub>2</sub> & volatile organic compounds) uncertainty was not  
8 elucidated. This paper (as an extension of Tang et al (2011)), based on the assimilation experiments  
9 performed by Tang et al., (2011), attempts to analyze in detail the impacts of the cross-variable ozone  
10 data assimilation on NO<sub>2</sub> forecasts over Beijing and surrounding areas during the 2008 Beijing  
11 Olympic Games. Both real O<sub>3</sub> data assimilation (with a 3-dimensional chemical transport model) and  
12 ideal O<sub>3</sub> data assimilation experiments (with a box model) are performed to investigate the state of  
13 NO<sub>2</sub> and NO<sub>x</sub> emissions during assimilation processes in order to provide further insights into the  
14 scientific potential of the assimilation method.

15 Section 2 describes the chemical transport model employed, the data assimilation algorithm and  
16 the surface observation network. Results from the real data assimilation experiments and the ideal  
17 data assimilation experiments are presented in Sect. 3. Section 4 presents conclusions and discussion.

## 18 **2. Methodology**

### 19 **(1) Chemical transport model**

20 The chemical transport model used for O<sub>3</sub> simulations was the Nested Air Quality Prediction  
21 Modeling System (NAQPMS) (Wang et al., 2001). Several applications of NAQPMS have been  
22 reported for simulating the chemical processes and transports of ozone, modeling the processes of  
23 aerosol and acid rain, and providing operational air quality forecasts in megacities such as Beijing  
24 and Shanghai (Wang et al., 2006). It contains modules for modeling the processes of emissions,  
25 advection, diffusion, dry and wet deposition, gaseous phase, aqueous phase, heterogeneous and  
26 aerosol chemical reactions. The gas-chemistry processes were simulated by the Carbon-Bond  
27 Mechanism Z (CBM-Z) which includes 133 reactions for 53 species (Zaveri and Peter, 1999). The  
28 dry deposition modeling followed the scheme of Wesely (1999). The vertical eddy diffusivity was  
29 parameterized based on a scheme by Byun and Dennis (1995). The O<sub>3</sub> simulations were configured

1 with three nested domains and the horizontal resolutions were 81km, 27km and 9km respectively.  
2 The first domain covered East Asia with a 81km resolution and the second domain contained North  
3 China with a 27km resolution. The third domain displayed in Fig. 1 covered Beijing and its  
4 surrounding areas with 9km resolution. Vertically, the model was set as twenty terrain-following  
5 layers, nine of which were within the lowest 2 km of the atmosphere and the height of the first layer  
6 near the surface was 50 m. The Fifth-Generation National Center for Atmospheric Research  
7 (NCAR)/Penn State Mesoscale Model (MM5; Grell et al., 1994) was employed to provide the hourly  
8 meteorological inputs for NAQPMS. The regional emission data of the Intercontinental Chemical  
9 Transport Experiment-Phase B (INTEX-B) Asia inventory for 2006 with  $0.5^\circ \times 0.5^\circ$  resolution  
10 (Zhang et al., 2009) and the local high-resolution emission inventory were combined to provide the  
11 emission data for NAQPMS (Tang et al., 2011).

## 12 **(2) Data assimilation algorithm**

13 The assimilation algorithm employed was the ensemble Kalman filter (EnKF) proposed by  
14 Evensen (1994). The main feature of this method consists of a series of ensemble samples generally  
15 produced via ensemble forecasts to calculate the background error covariance of state variables. It  
16 serves as an approximate version of the Kalman filter (Kalman, 1960). EnKF can directly calculate  
17 the background error covariance from the ensemble forecasts of the highly nonlinear model, which is  
18 very suitable for data assimilation in complex high-dimensional models (Carmichael et al., 2008). Its  
19 implementation is very simple and does not require an adjoint model which is a very cumbersome  
20 task for complex high-dimensional model. It can be used for combined state and parameter  
21 estimation (Evensen, 2009). In the field of air pollution, the EnKF has been shown to be an efficient  
22 method in optimizing concentrations. Further applications of the EnKF in improving dust and ozone  
23 forecast skills through emission optimization have been reported (e.g., Constantinescu et al., 2007;  
24 Eben et al., 2005; Lin et al., 2008; Tang et al., 2011).

25 In the present study, the EnKF was employed to assimilate ozone observations for the  
26 corrections of NO<sub>x</sub> emissions. The main purpose is to elucidate the performances of that method  
27 during the cross-variable assimilation of O<sub>3</sub> observations. The sequential algorithm proposed by  
28 Houtekamer and Mitchell (2001), as a variant of EnKF, was adopted for its efficiency in computation.  
29 The first step of the implementation was to perturb ozone concentrations, NO<sub>x</sub> emissions and other  
30 key uncertainty sources of ozone modeling, i.e., photolysis rates and vertical diffusion coefficients, as

1 described by the following equations:

$$2 \quad \mathbf{x}'(\mathbf{i}) = \mathbf{x}^b + \boldsymbol{\zeta}(\mathbf{i}), i = 1, 2, \dots, N \quad (1)$$

$$3 \quad \mathbf{e}'(\mathbf{i}) = \mathbf{e}^b + \boldsymbol{\varepsilon}(\mathbf{i}), i = 1, 2, \dots, N \quad (2)$$

$$4 \quad \mathbf{q}'(\mathbf{i}) = \mathbf{q}^b + \boldsymbol{\phi}(\mathbf{i}), i = 1, 2, \dots, N \quad (3)$$

5 where  $\mathbf{x}$ ,  $\mathbf{e}$ , and  $\mathbf{q}$  are ozone concentrations, emissions, and other parameters (NO<sub>2</sub> photolysis rates  
6 and vertical diffusion coefficients) respectively, and the superscript  $b$  represents their background  
7 values in the model. The superscript ' represents the ensemble samples of these variables after  
8 perturbing the background values by random samples of  $\boldsymbol{\zeta}$ ,  $\boldsymbol{\varepsilon}$ , and  $\boldsymbol{\phi}$ . The random samples were  
9 extracted from a normal distribution using the method proposed by Evensen (1994).  $N$  is the  
10 ensemble size. The ensemble size (set as 50) was chosen based on several sensitivity  
11 experiments of ozone data assimilation. The experiments were performed with the same model  
12 domains and observation network as those employed in this study. The results suggest that an  
13 ensemble of 50 members keeps good balance between computational efficiency and  
14 assimilation performance of ozone analysis.

15 In order to avoid filter divergence, the NO<sub>2</sub> photolysis rate and vertical diffusion coefficient  
16 were perturbed by Gaussian distributed random noise, and the NO<sub>x</sub> emissions (to be updated  
17 by the EnKF) were perturbed by a time-correlated Gaussian distributed random noise.  
18 Estimating the uncertainty of the NO<sub>x</sub> emissions used for the modeling during the Beijing Olympic  
19 Games was a hard task. The INTEX-B Asia inventory (Zhang et al., 2009) was estimated to contain  
20 31% uncertainty in NO<sub>x</sub> emission estimation. But the base year of this inventory is 2006. Another  
21 key factor affecting the emission uncertainty is the temporary air pollution control measures during  
22 the Beijing Olympic Games. The control measures were estimated to reduce the NO<sub>x</sub> emissions by  
23 36% to 47% (Wang et al., 2009; 2010). This would induce large biases into the emission inventory  
24 and lead to significant increase of the uncertainties of the emission inventory. Therefore, we  
25 estimated the uncertainty of the NO<sub>x</sub> emissions to be 60 % of the first guess emission rates, about  
26 twice the uncertainty in the INTEX-B Asia inventory. The uncertainties of vertical diffusion  
27 coefficients in ozone modeling have been estimated by Beekmann and Derognat (2003), Hanna et al.  
28 (1998) and Moore et al. (2001), ranging from 25% to 50%. We estimated the uncertainty of vertical  
29 diffusion coefficients to be 35% of the first guess values which are close to the average estimation of

1 the above three estimations. Also with reference to the studies of Hanna et al. (1998) and Moore et al.  
 2 (2001), the uncertainty of the modeled photolysis rates was estimated to be 30%. The uncertainty of  
 3 the modeled O<sub>3</sub> concentrations at the initial time was estimated to be 50% after comparing the  
 4 modeled O<sub>3</sub> concentrations with observations. Based on the method suggested by Evensen (1994),  
 5 the perturbations of the variables in three dimensions were implemented through adding a pseudo  
 6 smooth random field. The random samples were Gaussian distributed with zero mean. The horizontal  
 7 and vertical scales of initial error correlations could be effectively controlled using this method. The  
 8 scales were set as 54 km in the horizontal and 3 model grids in the vertical (approximately 200 m) as  
 9 in Tang et al. (2011).

10 Ensemble samples of the emissions, the vertical diffusion coefficients, the photolysis rates and  
 11 the O<sub>3</sub> concentrations were used to derive ensemble forecasts of ozone. In order to achieve  
 12 cross-variable adjustment for NO<sub>x</sub> emissions, an extended state variable was defined as:

$$13 \quad \mathbf{U}'(i) = \begin{bmatrix} \mathbf{x}'(i) \\ \mathbf{e}'(i) \end{bmatrix}, i = 1, 2, \dots, N \quad (4)$$

14 where  $\mathbf{x}'(i)$  and  $\mathbf{e}'(i)$  represent the ozone concentrations and the emissions after perturbations as  
 15 in Eq. (1). Through the ensemble forecast  $\mathbf{x}'(i)$  is strongly dependent on  $\mathbf{e}'(i)$ , which makes it  
 16 convenient for estimating the correlation between  $\mathbf{x}$  and  $\mathbf{e}$  and for cross-variable adjustment of NO<sub>x</sub>  
 17 emissions. The background error covariance of the extended variable could be directly calculated  
 18 from the ensemble forecast results during the simulation period:

$$19 \quad \mathbf{P} = \frac{1}{N-1} \sum_{i=1}^N (\mathbf{U}'(i) - \overline{\mathbf{U}'}) (\mathbf{U}'(i) - \overline{\mathbf{U}'})^T \quad (5)$$

20 where  $\overline{\mathbf{U}'}$  is the mean of the ensemble samples of the extended state variable and N is the ensemble  
 21 size.

22 This algorithm treats the observations as random variables and perturbs them to prevent filter  
 23 divergence of the EnKF (Houtekamer and Mitchell, 1998). When ozone observations are available,  
 24 they were perturbed according to the observation errors (Gaussian with mean zero and covariance  $\mathbf{R}$ ,  
 25 including both measurement errors and representativeness errors):

$$26 \quad \mathbf{y}'(i) = \mathbf{y} + \mathbf{Y}(i), i = 1, 2, \dots, N \quad (6)$$

$$27 \quad \mathbf{Y} \in N(0, \mathbf{R}).$$

28 As suggested by von Loon et al. (2000), the observation errors were assumed to be within 10% of the

1 original observation value and uncorrelated in time and space. It is worth noting that some other  
2 variants of the EnKF (e.g., the ensemble square root filter (EnSRF) proposed by Whitaker and Hamill,  
3 2002) do not need the perturbations on observations but can also provide accurate analyses.

4 Then the ensemble samples of the extended variables from the ensemble forecasts could be  
5 updated through assimilating the ozone observations:

$$6 \quad \mathbf{U}^a(\mathbf{i}) = \mathbf{U}'(\mathbf{i}) + \mathbf{K}(\mathbf{y}'(\mathbf{i}) - \mathbf{H}\mathbf{U}'(\mathbf{i})), \mathbf{i} = 1, 2, \dots, N \quad (7)$$

$$7 \quad \mathbf{K} = \mathbf{P}\mathbf{H}^T(\mathbf{H}\mathbf{P}\mathbf{H}^T + \mathbf{R})^{-1} \quad (8)$$

8 where  $\mathbf{H}$  represents a linear operator mapping the extended state variable from model space to  
9 observational space, and  $\mathbf{K}$  is the Kalman weight calculated based on the background error  
10 covariance and the observation error covariance.  $\mathbf{U}^a(\mathbf{i})$  is the updated ensemble sample of the  
11 extended state variable and was used for the sequential ozone forecast. The updating of the ensemble  
12 ensembles of the extended variables was conducted one time every 1 hour (1h), and the updated NOx  
13 emissions were then used for the NO<sub>2</sub> forecast of the next hour. The ensemble mean of  $\mathbf{U}^a(\mathbf{i})$  was  
14 taken as the best estimation after assimilating observations and was used as the output analysis state  
15 for comparisons (e.g. the blue dots in Figures 4 and 5). To reduce the spurious impact caused by  
16 the finite ensemble size, localization was performed for analysis and only observations within a  
17 localization scale were used to update the NOx emissions at a model grid. The localization scale  
18 was set as 45km following the configuration of Tang et al. (2011).

### 19 **(3) Surface observation network**

20 We employed a regional surface air quality network over Beijing and its surrounding areas  
21 during the 2008 Beijing Olympic Games including 17 stations established by the Beijing  
22 Environment Monitoring Center and Chinese Academy of Science (Xin et al., 2010). Figure 1  
23 displays the distributions of these stations and the non-industrial NOx emission rates of the  
24 observation regions in the third model domain. As can be seen, 11 urban stations (CP, PEK, BY, IAP,  
25 YF, BD, CZ, QHD, SJZ, TS, TJ) are located in the urban areas with high non-industrial NOx  
26 emission rates, and the other 6 (LF, XH, XL, YJ, YuF, YLD) are in the suburban areas with relatively  
27 low non-industrial NOx emission rates. The network provides observations of O<sub>3</sub> and NO<sub>2</sub> at the  
28 same temporal resolution as the model (i.e., 1h). The measurements of NO<sub>2</sub> and O<sub>3</sub> were observed by  
29 online instruments (Model 42C& 42I NO-NO<sub>2</sub>-NOx Analyzer and Model 49C&49I O<sub>3</sub> Analyzer

1 from Thermo Scientific). The O<sub>3</sub> observations were assimilated hourly into the model to adjust NO<sub>x</sub>  
2 emissions. The direct comparison between the simulated and observed NO<sub>2</sub> data often suffered from  
3 the representativeness errors of the NO<sub>2</sub> measurements. In this study, the stations close to the main  
4 roads with heavy traffic were not included in order to reduce the influence of the representativeness  
5 errors of the NO<sub>2</sub> measurements. Nevertheless, under certain resolutions (9km for example), the  
6 representativeness errors still persisted in NO<sub>2</sub> measurements over urban areas. In order to  
7 independently validate the assimilation results, three of the observation stations were withdrawn from  
8 the assimilation and were used for the validation. NO<sub>2</sub> observations not used in the assimilation were  
9 also used to assess the impacts of the cross-variable assimilation on the NO<sub>2</sub> forecasts.

### 10 **3. Results**

#### 11 **3.1 Real data assimilation experiment**

12 The real data assimilation (RDA) experiment assimilated the surface ozone observations over Beijing  
13 and surrounding areas to adjust the NO<sub>x</sub> emissions over these areas in the NAQPMS. The experiment  
14 was based on the study of Tang et al. (2011) in which the assimilation of real O<sub>3</sub> observations with  
15 the EnKF was performed to correct NO<sub>x</sub> emissions. The experiment focused on a two-week period  
16 from 00:00 LT 9 August to 00:00 LT 23 August in 2008. The initial conditions of the simulation  
17 were from a two-week spin-up model run. The initial conditions of ozone, NO<sub>x</sub> emissions and  
18 vertical diffusion parameters were perturbed at 19:00 LT on 8 August 2008 according to the  
19 equations (1), (2) and (3) and were used to derive ensemble runs of NAQPMS. After 5h free  
20 ensemble runs, the observed ozone data started at 00:00 LT on 9 August to be assimilated hourly into  
21 the third model domain (displayed in Fig. 1) of NAQPMS to adjust the NO<sub>x</sub> emissions. Adjusted  
22 factors of the NO<sub>x</sub> emissions were then used for the NO<sub>2</sub> forecast of the next hour. Both daytime and  
23 nighttime observations were assimilated. By considering possible large errors in the modeling of  
24 vertical profiles of air pollutants, we only adjust the variables in the first three vertical layers near the  
25 surface, which could reduce the influence of the modeling errors of vertical mixing on data  
26 assimilation. A free run of NAQPMS without data assimilation (NonDA) was also performed as a  
27 reference run to validate the assimilation results of the RDA experiment.

28 Figure 2 compares the root mean square errors (RMSEs) of the 1 h ensemble mean forecast of  
29 NO<sub>2</sub> at the 17 stations in the RDA experiment with the RMSEs in the NonDA experiment. The



1 RMSE of each site was calculated based on the hourly differences between NO<sub>2</sub> observation and the  
2 ensemble mean forecast of NO<sub>2</sub> from 00:00 LT 9 August to 00:00 LT 23 August in 2008. The  
3 number of valid observations used for each station is listed in Figure 2. The differences of the  
4 RMSEs before and after DA were statistically significant over 11 stations (TJ, BY, YF, IAP, CP, XH,  
5 CZ, PEK, QHD, SJZ and TS) at the 95% level of the t-test, while there were no statistically  
6 significant differences of the RMSEs before and after DA over 6 stations (XL, YuF, YJ, YLD, LF  
7 and BD). The RMSEs of the NO<sub>2</sub> forecasts in the free run of the model were dominated by the biases  
8 which accounted for 55~90% of the RMSEs (Bias/RMSE). Biases noticed in simulations performed  
9 over urban sites are relatively larger than those over the suburban ones. The free model run  
10 overestimated NO<sub>2</sub> concentrations at most of the urban stations, while underestimated it at most of  
11 the suburban ones. The DA impacts on the NO<sub>2</sub> forecast varied substantially from the suburban to the  
12 urban stations. At urban station such as BD, PEK, CZ, QHD, SJZ, and TS, the RMSEs were reduced  
13 by 15%~36% after DA, resulting in improvement of NO<sub>2</sub> forecasts in contrast to large increases,  
14 ranging from 56~239% of the RMSEs at CP, BY, IAP, YF and TJ. At the suburban sites, the DA  
15 showed minor influence on NO<sub>2</sub> forecasts and had no statistically significant impacts on the RMSEs  
16 over 5 of the 6 suburban sites. Such minor DA impacts over the suburban sites could be explained  
17 firstly, by the fact that emission rates of NO<sub>x</sub> in the model were very low over suburban regions and  
18 the simulation without DA significantly underestimated the NO<sub>2</sub> concentrations. Even with the  
19 perturbations on the NO<sub>x</sub> emission, the ensemble spread was significantly weaker than the errors in  
20 the real case, and thereby reduced the DA impacts of the EnKF. On the other hand, in regards to the  
21 influences of the air pollutants transport from urban regions, observed negative DA impacts over  
22 some urban areas may have induced significant errors into the NO<sub>2</sub> forecasts. The above results  
23 suggest the adjustment of the NO<sub>x</sub> emission by the ozone data assimilation has a mixed effect on the  
24 NO<sub>2</sub> forecast (i.e., weak DA impacts over suburban sites, positive DA impacts over some urban sites  
25 and negative DA impacts over others). Nevertheless, the assimilation produced significant  
26 improvement of ozone forecasts over all these sites, as reported by Tang et al. (2011).

27 Further investigations were conducted on the variation of such mixed effects of the data  
28 assimilation on NO<sub>2</sub> forecasts over both first week (from 00:00 LT 9 August to 00:00 LT 16 August  
29 in 2008) and second week (from 00:00 LT 16 August to 00:00 LT 23 August in 2008). As a result,  
30 the DA mixed effects were relatively stable during the Beijing Olympic Games. Figures 3 (a-c)

1 display daily variation of the 1h NO<sub>2</sub> forecast RMSEs in RDA experiment and NonDA experiment  
2 over the urban stations with positive DA impacts (CZ, PEK, QHD, SJZ, and TS), those with negative  
3 DA impacts (BY, CP, IAP, TJ and YF) and the suburban stations (LF, XH, YLD, YJ and YuF with  
4 weak DA impacts). At the suburban stations, the cross-variable DA also showed very weak impacts  
5 on the NO<sub>2</sub> forecast in both the daytime and nighttime. At the urban stations with positive DA  
6 impacts, the cross-variable assimilation presented consistent positive DA impacts in daytime,  
7 nighttime and morning, with a 23% reduction of RMSEs during daytime and a 21% reduction in  
8 night and morning.

9 At the urban sites with negative DA impacts, the performance of the DA was different between  
10 daytime, nighttime and morning hours. Adjusting NO<sub>x</sub> emissions improves the forecasts of NO<sub>2</sub>  
11 concentrations during most of the night and the morning time by reducing 7% of the RMSEs in  
12 contrast to the deterioration of the forecast in the daytime with 190% increase of the RMSEs. This  
13 finding suggests that the impacts of the cross-variable assimilation on the NO<sub>2</sub> forecast during  
14 daytime are opposite to those in night and morning at these urban sites. In clear, negative DA impacts  
15 mainly occur in the daytime. As described by Tang et al. (2010b), daytime ozone is strongly  
16 nonlinearly related to high NO<sub>x</sub> emissions over urban areas (in particular over central Beijing),  
17 whereas nighttime ozone is mainly controlled by the titration reaction of O<sub>3</sub>-NO with weak  
18 nonlinearity. Due to the obvious discrepancy between daytime ozone and nighttime ozone chemistry,  
19 further experiments were carried out in following section to elucidate the impact of the chemistry on  
20 the cross-variable assimilation.

21 Another phenomenon observed in Figs. 3(a-b) is that the errors in NO<sub>2</sub> forecasts with the free  
22 model run in night and morning were much higher than those in daytime. This might due to the large  
23 uncertainties in modeling of nighttime boundary layer over urban regions (Kleczek et al., 2014).  
24 Although the modeling of vertical diffusion was taken as a key uncertainty source in our data  
25 assimilation, its uncertainty was not constrained by the data assimilation. Therefore, high errors still  
26 subsisted in the nighttime NO<sub>2</sub> forecasts after data assimilation, as shown in Figs. 3(a-b).

### 27 **3.2 Ideal data assimilation experiment**

28 An ideal experiment with a known true state provided a simple way to investigate the potential  
29 consequences of some key inspected factors in a highly complex system. In order to investigate the

1 possible cause of observed mixed effects in RDA experiment, this study employed a simplified box  
2 model including the main chemical processes of NAQPMS (Xiang et al., 2010). Within conducted  
3 ideal data assimilation (IDA) experiments, the true state of ozone concentrations and NO<sub>x</sub> emissions  
4 were assumed to be known. The main purpose is to closely monitor the impacts of ozone chemistry  
5 on the cross-variable assimilation method experimented in the RDA. However, this investigation did  
6 not take into account complex transport processes and the removal processes were simulated by  
7 multiplying the concentrations by removal coefficients. The experiments with the box model were  
8 conducted on the IAP station where negative impact on NO<sub>2</sub> forecasts is observed in the RDA  
9 experiment. Emission rates and meteorological parameters are from the inputs used by NAQPMS.

10 Firstly, the IDA experiments focused on the negative DA impacts on the daytime NO<sub>2</sub> forecasts.  
11 The a priori emission rates from NAQPMS and their corresponding O<sub>3</sub> concentrations modeled with  
12 the box model were assumed to be the true state and were used for validation of the optimized  
13 emissions from DA. Ensemble runs of the box model were initialized by the ensemble forecasts of the  
14 chemical species of NAQPMS at 19:00 LT on 11 August 2008; NO<sub>x</sub> emissions were perturbed to  
15 provide ensemble samples of emissions during the following ensemble runs of the model. At 12:00 LT  
16 on 12 August 2008, the artificial O<sub>3</sub> observation was assimilated into the box model to adjust the NO<sub>x</sub>  
17 emissions. Artificial O<sub>3</sub> observations were generated through adding slight random errors to the true  
18 state of O<sub>3</sub> concentrations. To be consistent with the RDA experiment, the random errors for perturbing  
19 observations were also assumed to be within 10% of the true value. Three error scenarios for NO<sub>x</sub>  
20 emissions (10%, 30% and 50% underestimations) were assumed and separately applied to simulations  
21 of the box model. In order to avoid dealing with complex model errors, the errors in NO<sub>x</sub> emissions  
22 were assumed to be the only error sources of ozone modeling. For each error scenario, cross-variable  
23 adjustment of the NO<sub>x</sub> emissions through assimilating the artificial O<sub>3</sub> observations with the EnKF  
24 was conducted. Figures 4(a-c) show the O<sub>3</sub> concentrations and NO<sub>x</sub> emissions before and after DA,  
25 with their ensemble samples before DA at 12:00 August 12, 2008.

26 Figure 4a presents the results under the first scenario with 10% underestimation of NO<sub>x</sub>  
27 emissions (S1). The analyzed O<sub>3</sub> concentration and NO<sub>x</sub> emission after DA were close to their true  
28 state, suggesting an improvement of the NO<sub>x</sub> emission estimation from the cross-variable assimilation.  
29 Figure 4b shows the results under the second scenario with 30% underestimation of NO<sub>x</sub> emissions  
30 (S2). The DA inefficiently reduced the error in NO<sub>x</sub> emission, since large errors (about 20%) still

1 persisted in the optimized NO<sub>x</sub> emission. Ensemble samples of O<sub>3</sub> concentrations shown in Fig.4b  
2 were obtained from the ensemble runs of the box model that were derived from the ensemble samples  
3 of NO<sub>x</sub> emissions (also shown in Fig.4b). Obviously, the ensemble forecasts of O<sub>3</sub> concentrations  
4 presented high nonlinear responses to the perturbations of NO<sub>x</sub> emissions. This suggests that the EnKF  
5 with Monte Carlo simulations can properly predict the nonlinear evolutions of error statistics of the O<sub>3</sub>  
6 modeling. At the analysis step, the ensemble samples of O<sub>3</sub> concentrations and NO<sub>x</sub> emissions were  
7 integrated into the EnKF to calculate the background error covariance in Eq. (5). The linearized  
8 relationship between the O<sub>3</sub> concentrations and the NO<sub>x</sub> emissions is presented in Fig. 4b. Noticeable  
9 discrepancies appear between the nonlinear relationship denoted by the ensemble samples and the  
10 linearized relationship at the analysis step. This significantly weakens the performance of the EnKF in  
11 the cross-variable adjustment.

12 In the third scenario (S3) with NO<sub>x</sub> emissions underestimated by 50%, enhanced deterioration of  
13 the NO<sub>x</sub> emission estimations was observed (Fig. 4c). The DA closely adjusted the simulated O<sub>3</sub>  
14 concentration to the true state, but induced additional bias to previously underestimated NO<sub>x</sub> emission.  
15 Such negative DA impact on NO<sub>x</sub> emission estimation was similar to the phenomenon observed on the  
16 daytime NO<sub>2</sub> forecast over some urban stations in the RDA experiment. From the results in Fig. 4(a-c),  
17 the most plausible cause of the negative DA impact on NO<sub>x</sub> emission estimation is the linearizing  
18 analysis of the EnKF in dealing with the cross-variable (O<sub>3</sub> to NO<sub>x</sub> emission) DA problem of a highly  
19 nonlinearly chemical system. With large bias in the a priori estimation of NO<sub>x</sub> emissions, the  
20 cross-variable assimilation may induce enhancement of the bias in NO<sub>x</sub> emissions. The results of the  
21 three IDA experiments (i.e., positive DA impact under the first and second scenarios and negative  
22 impact under the third scenario) confirm the mixed effects of the cross-variable assimilations observed  
23 in the RDA experiments, and suggest a strong link between the mixed effects and the linearization  
24 process at the analysis step of the EnKF over strongly nonlinear chemical system.

25 In order to consider error scenarios with overestimations of NO<sub>x</sub> emission, four idealized DA  
26 experiments in which NO<sub>x</sub> emission was assumed to being overestimated by 10%, 30%, 50% and 100%  
27 respectively were performed. The results are shown in Fig. 5(a-d). In the first three experiments with  
28 10%, 30% and 50% overestimations of the a priori NO<sub>x</sub> emission, the DA worked well and  
29 significantly reduced the biases of the emission. In the fourth experiment with the largest bias in the a  
30 priori emission estimation, the DA enhanced the bias of the emission estimation in daytime. These

1 mixed DA effects under different biases of the a priori emission estimation are similar to those  
2 observed in previous idealized experiments conducted with underestimate scenarios. Both  
3 underestimate and overestimate scenarios clearly confirm the mixed effects of the DA.

4 Note that above IDA experiments do not consider the complex model errors (e.g., errors in  
5 boundary layer or transport modeling). In the real case, model errors exist, and the DA scheme needs  
6 to properly quantify model uncertainties and deal with the nonlinearity between assimilated  
7 observations and adjusted variables simultaneously. Model errors may affect the results of the real DA.  
8 Thus, in order to investigate the DA performance of adjusting NO<sub>x</sub> emissions under the presence of  
9 biases on other factors, we assumed that the NO<sub>2</sub> photolysis rate was overestimated by 20% in the  
10 idealized box modeling, since the errors of the NO<sub>2</sub> photolysis rates were found to be the top five  
11 uncertainty sources of ozone modeling over Beijing and surrounding areas during the Beijing Olympic  
12 Games (Tang et al., 2010a).

13 Firstly, we were blind to the bias of the simulated NO<sub>2</sub> photolysis rate, so that no perturbation was  
14 operated on it in the DA experiment. The NO<sub>x</sub> emission was adjusted in the same way as the  
15 above-idealized experiments. Fig. 6a displays the results of the DA experiment under the error  
16 scenario of 30% overestimation in the a priori NO<sub>x</sub> emission. The DA corrected the NO<sub>x</sub> emission, but  
17 led to an underestimation of the emission. This over-correction of NO<sub>x</sub> emission by the DA could be  
18 associated with the bias in simulated NO<sub>2</sub> photolysis rate. Therefore, in the second experiment (Fig.  
19 6b), we considered the uncertainty of the simulated NO<sub>2</sub> photolysis rate and perturbed the NO<sub>2</sub>  
20 photolysis rate in the DA. The error scenario was the same as in the first experiment. Under that  
21 condition, the DA performed better than that of the first experiment, without over-correction of NO<sub>x</sub>  
22 emission. The results of above experiments suggest that considering the model errors is crucial for the  
23 assimilation performance; otherwise the DA leads to over-correction to the state variable. In order to  
24 deal with this issue, simulated NO<sub>2</sub> photolysis rates and vertical diffusion coefficients (considered as  
25 the key uncertainty sources of the O<sub>3</sub> modeling) were perturbed to account their uncertainties into the  
26 real DA experiment. The third DA experiment is quite similar to the second one, but we increased the  
27 bias of the a priori NO<sub>x</sub> emission to 100% overestimation. The results are shown in Fig. 6c. Under  
28 large bias in the a priori NO<sub>x</sub> emission, the DA deteriorated NO<sub>x</sub> emission estimation. In short, in  
29 sight of considering the influence of the model errors, the limitations of the DA method in dealing with  
30 the large bias of a highly nonlinear system are still persistent.

1 To investigate the DA impacts on the NO<sub>x</sub> emissions in night and morning, variations of O<sub>3</sub>  
2 concentrations and NO<sub>x</sub> emissions before and after DA and their ensemble samples before DA at 8:00  
3 August 13, 2008 (morning time) are shown in Figs. 7(a-c). Similar trends (not shown here) were  
4 obtained for other night and morning times. In Figs. 7(a-c), different level errors (10%, 30% and 50%  
5 underestimations) in NO<sub>x</sub> emissions were significantly reduced through the cross-variable assimilation  
6 with the EnKF. The ensemble forecasts of morning O<sub>3</sub> concentrations show near-linear responses to  
7 the uncertainties (or perturbations) of NO<sub>x</sub> emissions; the linearization of the EnKF at the analysis step  
8 worked properly to correct the biases in NO<sub>x</sub> emissions. The positive DA impacts on the NO<sub>x</sub>  
9 emission estimation in IDA experiments in night and morning were consistent with the improvement  
10 of the NO<sub>2</sub> forecasts after data assimilation in RDA experiment. In comparison with the mixed effects  
11 of the DA in daytime, the positive DA impacts in night and morning in both RDA and IDA  
12 experiments indicate that the assimilation of O<sub>3</sub> observations with the EnKF might be useful in  
13 optimizing NO<sub>x</sub> emissions and NO<sub>2</sub> forecasts in night and morning. Furthermore, the ensemble  
14 forecasts of O<sub>3</sub> concentrations show strong nonlinear responses to the perturbations of NO<sub>x</sub> emissions  
15 during daytime in Figs. 4(a-c) but present near-linear responses in night and morning in Figs. 7(a-c).  
16 This suggests the variability of nonlinearity of the chemical system leads to different DA impacts  
17 during different periods of the day.

#### 18 **4. Conclusion and discussion**

19 The impacts of cross-variable adjustment of NO<sub>x</sub> emissions on NO<sub>2</sub> forecasts were investigated  
20 through assimilating O<sub>3</sub> observations with a variant of the EnKF (proposed by Houtekamer and  
21 Mitchell, 2001) over Beijing and surrounding areas during the 2008 Beijing Olympic Games. Both  
22 real DA experiments with a 3-dimensional chemical transport model and ideal DA experiments with  
23 a simplified box chemical model were performed.

24 The results of the data assimilation experiments revealed mixed effects of the cross-variable  
25 assimilation with the EnKF. The DA worked properly in improving the NO<sub>2</sub> forecasts and optimizing  
26 the NO<sub>x</sub> emissions in night and morning when the uncertainties of O<sub>3</sub> concentrations were almost  
27 linearized to those of NO<sub>x</sub> emissions. During daytime, the data assimilation resulted in positive DA  
28 impacts on NO<sub>2</sub> forecasts over some urban sites, negative over other urban sites and weak impacts  
29 over suburban sites. Through idealized DA experiments, the mixed effects were found to be strongly

1 associated with the difficulty in dealing with highly nonlinear DA problem especially under large  
2 model biases. The results highlighted critical limitation of the EnKF for the chemical DA despite its  
3 strong performance for improving ozone forecasts (e.g., Tang et al., 2011).

4 The results suggest that bias correction is crucial for the application of the EnKF in highly  
5 nonlinear chemical DA problem. Alternatively, avoiding the cross-variable DA between two  
6 strong-nonlinearly related variables such as NO<sub>x</sub> emissions and O<sub>3</sub> is also a possible way to  
7 overcome this issue. For example, assimilating NO<sub>2</sub> observations directly to optimize NO<sub>x</sub> emissions  
8 might produce better result than assimilating O<sub>3</sub> observations to improve the NO<sub>2</sub> forecasts and NO<sub>x</sub>  
9 emission estimations. Nevertheless, strong nonlinearity issue remains a critical challenge in the  
10 chemical DA. In sum, DA approaches that enable dealing with high nonlinearity in both model  
11 evolution and analysis step are needed. Particle filters as nonlinear filter method (e.g., Moral et al.,  
12 1996; van Leeuwen, 2009; 2010) might have potential in this field if its limitation for high  
13 dimensional system application (Stordal et al., 2011) can be overcome.

#### 14 **Acknowledgements**

15 This study was funded by the CAS Strategic Priority Research Program (Grant No. XDB05030200)  
16 and the National Natural Science Foundation (Grant No. 41205091 and No. 41305111).

#### 17 **References**

- 18 Beekmann, M., Derognat, C.: Monte Carlo uncertainty analysis of a regional-scale transport  
19 chemistry model constrained by measurements from the Atmospheric Pollution Over the Paris  
20 Area (ESQUIF) campaign, *J. Geophys. Res.* 108, doi:10.1029/2003JD003391, 2003.
- 21 Byun, D.W., Dennis, R.: Design artifacts in Eulerian air quality models: evaluation of the effects of  
22 layer thickness and vertical profile correction on surface ozone concentrations, *Atmos. Environ.*  
23 29, 105–126, 1995.
- 24 Carmichael, G., Chai, T., Sandu, A., Constantinescu, E., Daescu, D.: Predicting air quality:  
25 Improvements through advanced methods to integrate models and measurements, *J. Comput. Phys.*  
26 227, 3540–3571, 2008.
- 27 Constantinescu, E.M., Sandu, A., Chai, T.F. and Carmichael, G.R.: Ensemble-based chemical data  
28 assimilation. II: Covariance localization, *Q. J. R. Meteorol. Soc.* 133: 1245–1256, 2007.
- 29 Eben, K., Jurus, P., Resler, J., Belda, M., Pelikan, E., Kruger, B. C., and Keder, J.: An ensemble  
30 Kalman filter for short-term forecasting of tropospheric ozone concentrations, *Q. J. R. Meteorol.*  
31 *Soc.* (2005), 131, 3313–3322, 2005.
- 32 Elbern, H., Strunk, A., Schmidt, H., Talagrand, O.: Emission rate and chemical state estimation by

- 1 4-dimensional variational inversion, *Atmos. Chem. Phys.* 7, 3749–3769, 2007.
- 2 Evensen, G.: Sequential data assimilation with a nonlinear quasi-geostrophic model using  
3 Monte-Carlo methods to forecast error statistics, *J. Geophys. Res.* 99, 10143-10162, 1994.
- 4 Gaubert, B., Coman, A., Foret, G., Meleux, F., Ung, A., Rouil, L., Ionescu, A., Candau, Y.,  
5 Beekmann, M.: Regional scale ozone data assimilation using an ensemble Kalman filter and the  
6 CHIMERE chemical transport model, *Geosci. Model. Dev.* 7, 283–302, 2014.
- 7 Grell, G.A., Dudhia, J., Stauffer, D.R.: A description of the fifth-generation Penn State/NCAR  
8 mesoscale model (MM5), NCAR Technical Note NCAR/TN-398+STR, 117 pp, 1994.
- 9 Hanea, R.G., Velders, G., Heemink, A.: Data assimilation of ground-level ozone in Europe with a  
10 Kalman filter and chemistry transport model, *J. Geophys. Res.* 109, doi:10.1029/2003JD004283,  
11 2004.
- 12 Hanna, S.R., Chang, J.C., Fernau, M.E.: Monte Carlo estimates of uncertainties in predictions by a  
13 photochemical grid model (UAM-IV) due to uncertainties in input variables, *Atmos. Environ.*,  
14 32(21), 3619-3628, 1998.
- 15 Hanna, S.R., Lu, Z.G., Frey, H.C., Wheeler, N., Vukovich, J., Arunachalam, S., Fernau, M., Hansen,  
16 D.A.: Uncertainties in predicted ozone concentrations due to input uncertainties for the UAM-V  
17 photochemical grid model applied to the July 1995 OTAG domain, *Atmos. Environ.* 35, 891-903,  
18 2001.
- 19 Houtekamer, P.L., Mitchell, H.L.: Data assimilation using an ensemble Kalman filter technique, *Mon.*  
20 *Wea. Rev.* 126, 796–811, 1998.
- 21 Houtekamer, P.L., Mitchell, H.L.: A sequential ensemble Kalman filter for atmospheric data  
22 assimilation, *Mon. Wea. Rev.* 129, 123–137, 2001.
- 23 Jimenez, P., Parra, R., and Baldasano, J. M.: Influence of initial and boundary conditions for ozone  
24 modeling in very complex terrains: A case study in the northeastern Iberian Peninsula,  
25 *Environmental Modelling & Software*, 22, 1294-1306, 2007.
- 26 Kleczek, M.A., Steeneveld, G., Holtslag, A.A.M.: Evaluation of the Weather Research and  
27 Forecasting mesoscale model for GABLS3: impact of boundary-layer schemes, boundary  
28 conditions and spin-up, *Boundary-Layer Meteorol.* 152, 213–243, 2014.
- 29 Koohkan, M.R., Bocquet, M., Roustan, Y., Kim, Y., Seigneur, C.: Estimation of volatile organic  
30 compound emissions for Europe using data assimilation, *Atmos. Chem. Phys.* 13, 5887–5905,  
31 2013.
- 32 Lin, C., J. Zhu, and Z. Wang: Model bias correction for dust storm forecast using ensemble Kalman  
33 filter, *J. Geophys. Res.*, 113, D14306, doi:10.1029/2007JD009498, 2008.
- 34 Moore, G.E., Londergan, R.J.: Sampled Monte Carlo uncertainty analysis for photochemical grid  
35 models, *Atmos. Environ.*, 35(28), 4863-4876, 2001.
- 36 Moral, P.D.: Nonlinear filtering: interacting particle solution, *Markov Processes and Related Fields*, 2  
37 (4), 555–580, 1996.

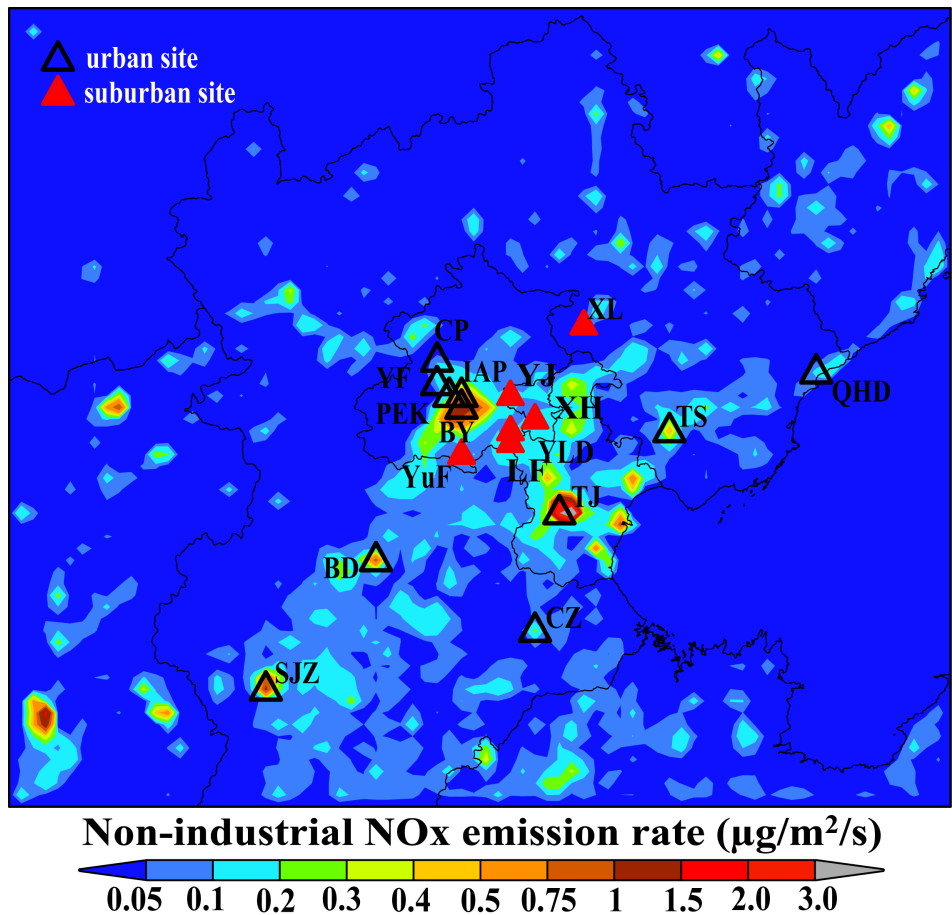


- 1 Pagowski, M., Liu, Z., Grell, G.A., Hu, M., Lin, H.-C., Schwartz, C.S.: Implementation of aerosol  
2 assimilation in Gridpoint Statistical Interpolation (v.3.2) and WRF-Chem (v.3.4.1), *Geosci. Model*  
3 *Dev.* 7, 1621–1627, 2014.
- 4 Sandu, A., Chai, T.: Chemical Data Assimilation—An Overview, *Atmosphere* 2, 426-463, 2011.
- 5 Stordal, A.S., Karlsen, H.A., Nævdal, G., Skaug, H.J., Vallès, B.: Bridging the ensemble Kalman  
6 filter and particle filters: the adaptive Gaussian mixture filter, *Comput. Geosci.* 15, 293–305,  
7 doi:10.1007/s10596-010-9207-1, 2011.
- 8 Tang, X., Wang, Z.F., Zhu, J., Wu, Q.Z., Gbaguidi, A.: Preliminary application of Monte Carlo  
9 uncertainty analysis in ozone simulation, *Clim. Environ. Res.* (in Chinese) 15 (5), 541-550, 2010a.
- 10 Tang, X., Wang, Z.F., Zhu, J., Gbaguidi, A., Wu, Q.Z., Li, J., Zhu, T.: Sensitivity of ozone to  
11 precursor emissions in urban Beijing with a Monte Carlo scheme, *Atmos. Environ.* 44, 3833-3842,  
12 2010b.
- 13 Tang, X., Zhu, J., Wang, Z.F., Gbaguidi, A.: Improvement of ozone forecast over Beijing based on  
14 ensemble Kalman filter with simultaneous adjustment of initial conditions and emissions, *Atmos.*  
15 *Chem. Phys.* 11, 12901-12916, 2011.
- 16 Tang, X., Zhu, J., Wang, Z.F., Wang, M., Gbaguidi, A., Li, J., Shao, M., Tang, G.Q., Ji, D.S.:  
17 Inversion of CO emissions over Beijing and its surrounding areas with ensemble Kalman filter,  
18 *Atmos. Environ.* 81, 676-686, 2013.
- 19 van Leeuwen P.J.: Particle filtering in geophysical systems, *Mon. Wea. Rev.* 137, 4089–4114, 2009.
- 20 van Leeuwen P.J.: Nonlinear data assimilation in geosciences: an extremely efficient particle filter, *Q.*  
21 *J. R. Meteorol. Soc.* 136, 1991–1999, doi:10.1002/qj.699, 2010.
- 22 van Loon, M., Builtjes, P., Segers, A.J.: Data assimilation of ozone in the atmospheric transport  
23 chemistry model LOTOS, *Environ. Model. Softw.* 15, 603–609, 2000.
- 24 Wang, S.X., Zhao, M., Xing, J., Wu, Y., Zhou, Y., Lei, Y., He, K.B., Fu, L.X., Hao, J.M.:  
25 Quantifying the Air Pollutants Emission Reduction during the 2008 Olympic Games in Beijing,  
26 *Environ. Sci. Technol.*, 44 (7), 2490–2496, 2010.
- 27 Wang, Y., Hao, J., McElroy, M. B., Munger, J. W., Ma, H., Chen, D., Nielsen, C. P.: Ozone air  
28 quality during the 2008 Beijing Olympics: effectiveness of emission restrictions, *Atmos. Chem.*  
29 *Phys.*, 9, 5237–5251, 2009.
- 30 Wang, Z., Maeda, T., Hayashi, M., Hsiao, L.F., Liu, K.Y.: A nested air quality prediction modeling  
31 system for urban and regional scales: application for high-ozone episode in Taiwan, *Water Air and*  
32 *Soil Pollution* 130, 391-396, 2001.
- 33 Wang, Z.F., Xie, F.Y., Wang, X.Q., An, J.L., Zhu, J.: Development and application of Nested Air  
34 Quality Prediction Modeling System, *Chinese Journal of Atmospheric Sciences* (in Chinese) 30,  
35 778–790, 2006.
- 36 Wesely, M.L.: Parameterization of surface resistances to gaseous dry deposition in regional-scale  
37 numerical models, *Atmos. Environ.* 23, 1293-1304, 1999.

- 1 Whitaker, J.S., Hamill, T.M.: Ensemble data assimilation without perturbed observations. *Mon. Wea.*  
2 *Rev.* 130, 1913–1924, 2002.
- 3 Wu, L., Mallet, V., Bocquet, M., Sportisse, B.: A comparison study of data assimilation algorithms  
4 for ozone forecasts, *J. Geophys. Res.* 113, D20310, doi:10.1029/2008JD009991, 2008.
- 5 Xiang, W.L., An, J.L., Wang, Z.F., Wu, Q.Z., Tang, X.: Application of CBM-Z chemical mechanism  
6 during Beijing Olympics, *Clim. Environ. Res.* (in Chinese) 15 (5), 551-559, 2010.
- 7 Xin, J.Y., Wang, Y.S., Tang, G.Q., Wang, L.L., Sun, Y., Wang, Y.H., Hu, B., Song, T., Ji, D.S.,  
8 Wang, W.F., Li, L., Liu, G.R.: Variability and reduction of atmospheric pollutants in Beijing and  
9 its surrounding area during the Beijing 2008 Olympic Games, *Chinese Sci. Bull.* (in Chinese) 55,  
10 1937–1944, 2010.
- 11 Zaveri, R.A., Peters, L.K.: A new lumped structure photochemical mechanism for large-scale  
12 applications, *J. Geophys. Res.* 104, 30387-30415, 1999.
- 13 Zhang, Q., Streets, D.G., Carmichael, G.R., He, K.B., Huo, H., Kannari, A., Klimont, Z., Park, I.S.,  
14 Reddy, S., Fu, J.S., Chen, D., Duan, L., Lei, Y., Wang, L.T., Yao, Z.L.: Asian emissions in 2006  
15 for the NASA INTEX-B mission, *Atmos. Chem. Phys.* 9, 5131-5153, 2009.
- 16 Zhang, Y., Bocquet, M., Mallet, V., Seigneur, C., Baklanov, A.: Real-time air quality forecasting,  
17 part II: State of the science, current research needs, and future prospects, *Atmos. Environ.* 60,  
18 656-676, 2012.

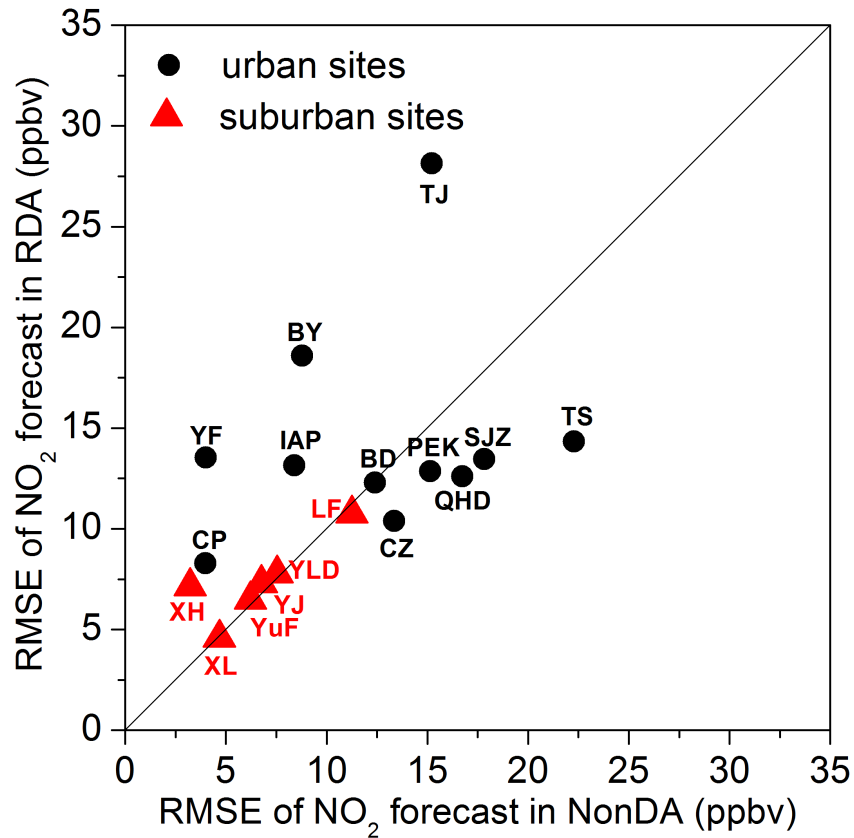
19

20 **Figures**



1  
2  
3  
4  
5  
6  
7  
8  
9  
10  
11

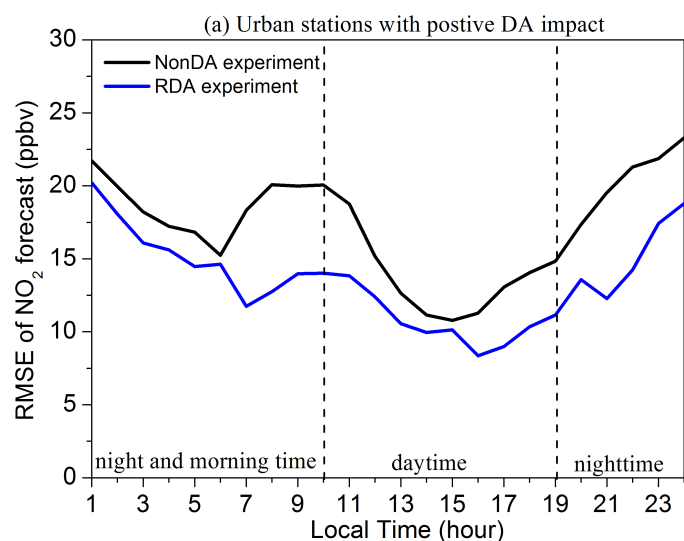
**Figure 1** Distribution of the observation stations and non-industrial NO<sub>x</sub> emission rates in the third model domain (9km resolution) that covers Beijing and its surrounding areas. The non-industrial NO<sub>x</sub> emission rates ( $\mu\text{g}/\text{m}^2/\text{s}$ ) are divided into different bins (<0.05; 0.01-0.1; 0.1-0.2; 0.2-0.3; 0.3-0.4; 0.4-0.5; 0.5-0.75; 0.75-1.0; 1.0-1.5; 1.5-2.0; 2.0-3.0) and represented by different shaded colors. The urban areas with high non-industrial NO<sub>x</sub> emission rates are marked by the brown and red colors, and the suburban or rural areas with low non-industrial NO<sub>x</sub> emission rates are marked by the green or blue colors. The 11 urban sites are denoted by the black triangles, and the 6 suburban stations are represented by the red triangles. The abbreviations of the station names are displayed close to the marks.



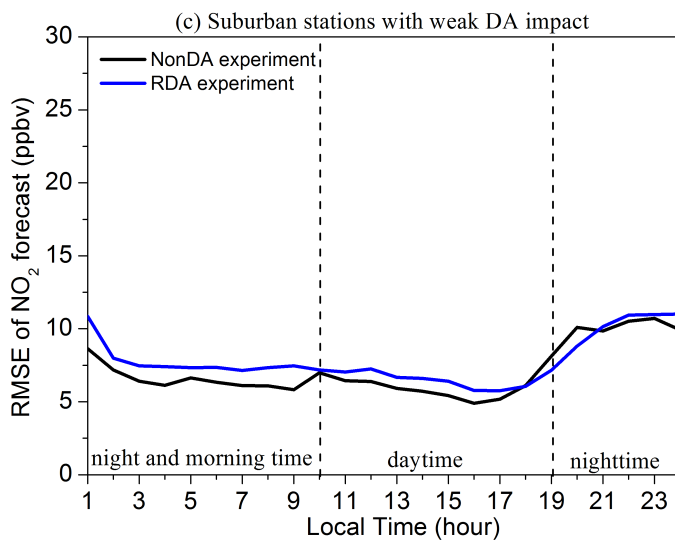
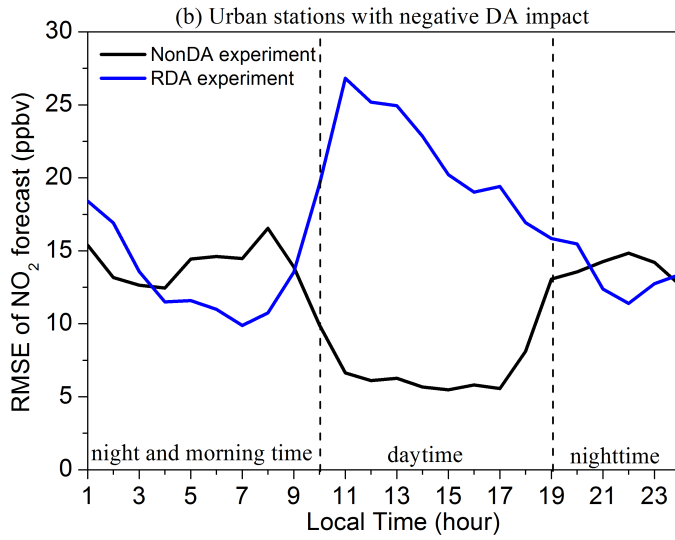
1

2 **Figure 2** Comparison of the root mean square errors (RMSEs) (ppbv) of 1h NO<sub>2</sub> forecasts at the 17  
 3 stations of Beijing and its surrounding areas during the period of 00:00 LT 9 August to 00:00 LT 23  
 4 August in 2008 in the real data assimilation (RDA) experiments and those in the reference (NonDA)  
 5 experiment with a free run of the model. The comparisons at urban sites are denoted by the dots and  
 6 those over suburban stations are represented by the triangles. The abbreviations of the station  
 7 names are displayed close to the marks. The number of the valid observations used for the  
 8 calculation is 336 at QHD, SJZ, TS, IAP, LF, YF and XH, and the numbers are 292, 226, 326, 317,  
 9 326, 320, 333, 321, 311, 323 at BD, PEK, BY, CZ, CP, TJ, XL, YJ, YLD and YuF respectively.

10



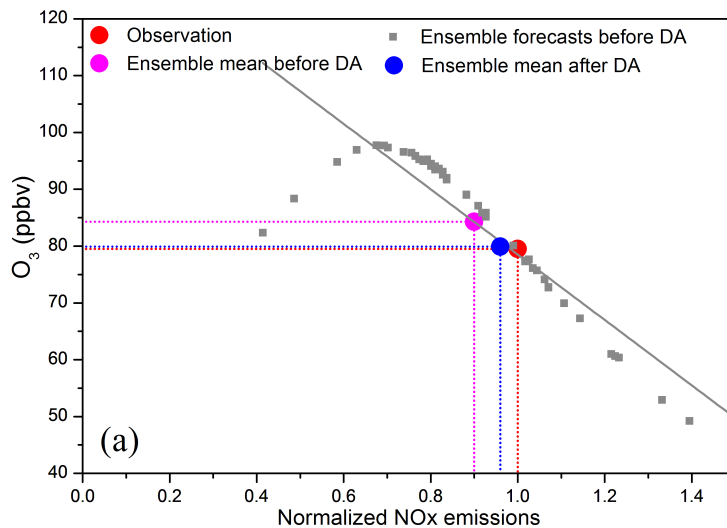
11



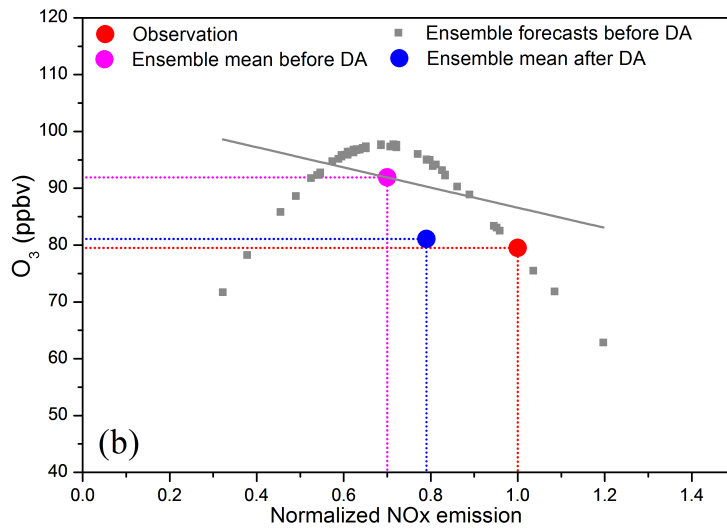
1

2

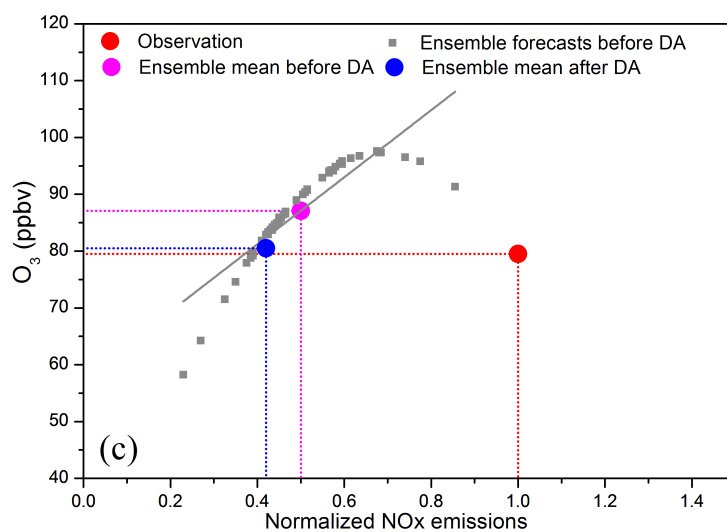
3 **Figure 3** Daily variation of the 1h NO<sub>2</sub> forecast RMSEs (ppbv) in the real data assimilation (RDA)  
 4 experiments (blue line) and the reference (NonDA) experiment with a free run of the model (black  
 5 line) over: (a) urban stations (CZ, PEK, QHD, SJZ, and TS) with positive DA impacts; (b) urban sites  
 6 (BY, CP, IAP, TJ and YF) with negative DA impacts; (c) suburban stations (LF, XH, YLD, YJ and  
 7 YuF) with weak DA impacts.



8



1

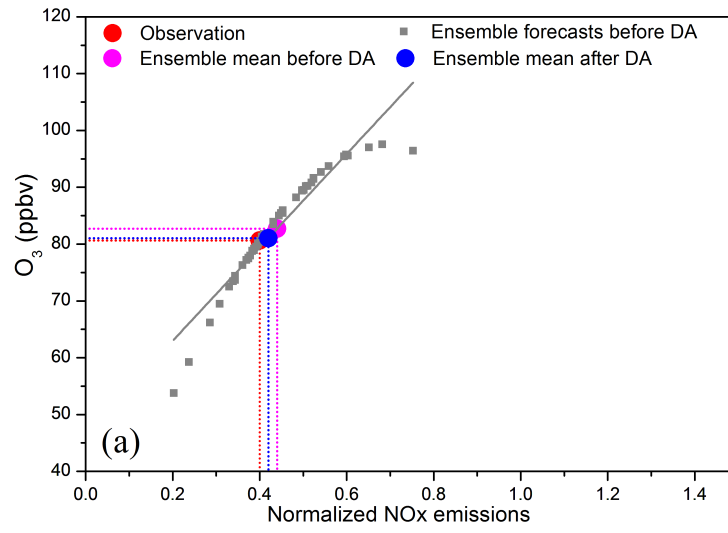


2

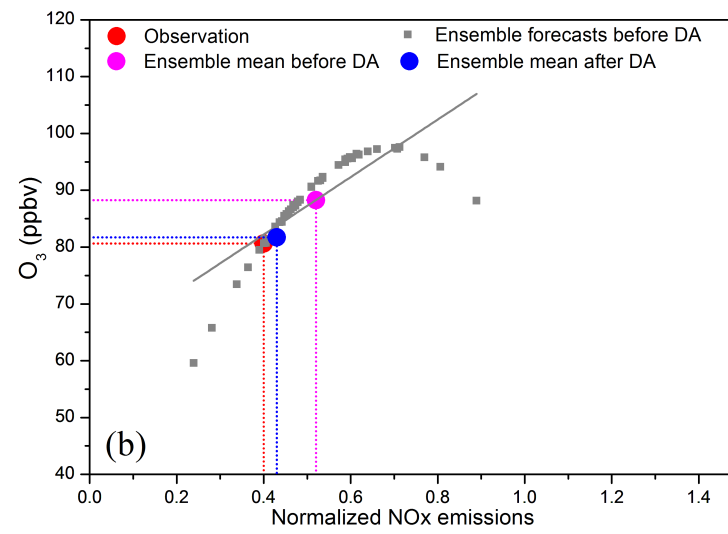
3 **Figure 4 (a-c)** O<sub>3</sub> concentrations (ppbv) and NO<sub>x</sub> emissions (no unit, normalized by the true NO<sub>x</sub>  
 4 emission) before and after data assimilation (DA) and their ensemble samples before DA at 12:00 LT  
 5 on August 12, 2008 in the three ideal ozone data assimilation experiments with the prior NO<sub>x</sub>  
 6 emissions underestimated by 10% (a), 30% (b) and 50% (c) respectively. The grey squares denote the  
 7 ensemble forecast O<sub>3</sub> concentrations corresponding to the perturbations of the NO<sub>x</sub> emissions  
 8 (ensemble forecasts before DA), and the magenta dot represents the result of the ensemble mean of  
 9 the grey squares (ensemble mean before DA). The gray line represents a linear relationship calculated  
 10 from the ensemble samples of O<sub>3</sub> concentrations and NO<sub>x</sub> emissions. The red dot represents the true  
 11 state of NO<sub>x</sub> emission and the observed O<sub>3</sub> concentration. The analyzed O<sub>3</sub> concentration and NO<sub>x</sub>  
 12 emission are denoted by the blue dot.

13

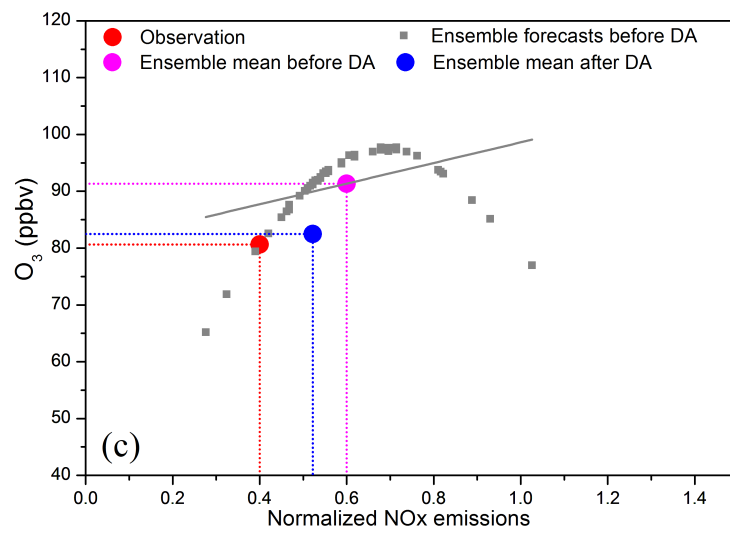
1

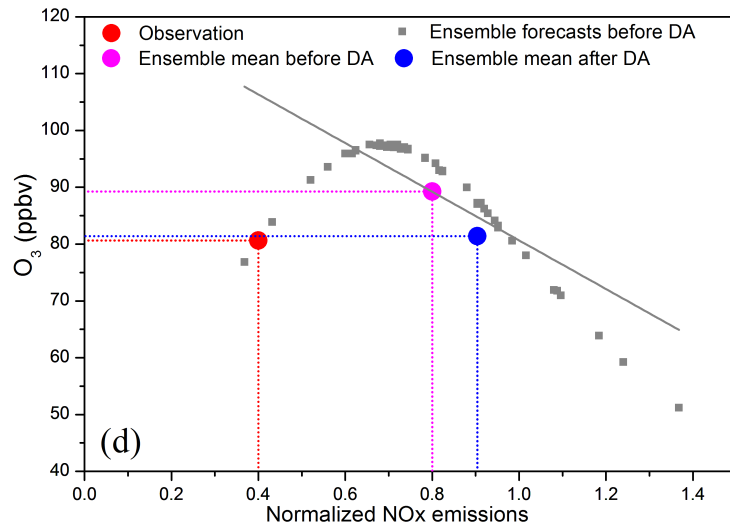


2



3





1

2

3

4

5

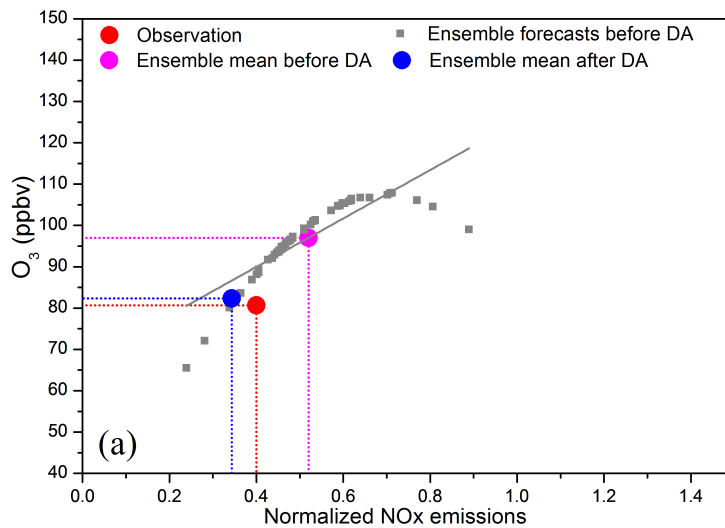
6

7

8

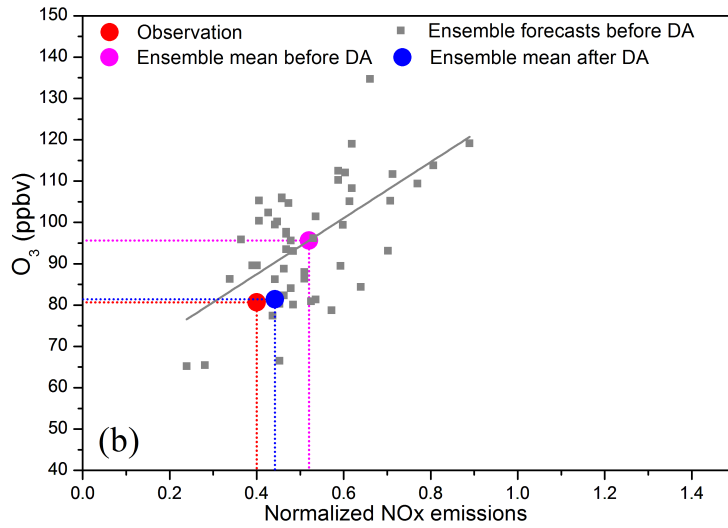
9

Figure 5 (a-d) O<sub>3</sub> concentrations (ppbv) and NOx emissions (no unit, normalized by the true NOx emission) before and after data assimilation (DA) and their ensemble samples before DA at 12:00 LT on August 12, 2008 in the four idealized DA experiments. (a) DA experiment with 10% overestimation in the a priori NOx emission estimation; (b) DA experiment with 30% overestimation in the a priori NOx emission estimation; (c) DA experiment with 50% overestimation in the a priori NOx emission; (d) DA experiment with 100% overestimation in the a priori NOx emission. The magenta dot, the gray squares, the gray line, the red dot and the blue dot represent the same as in Fig. 4.

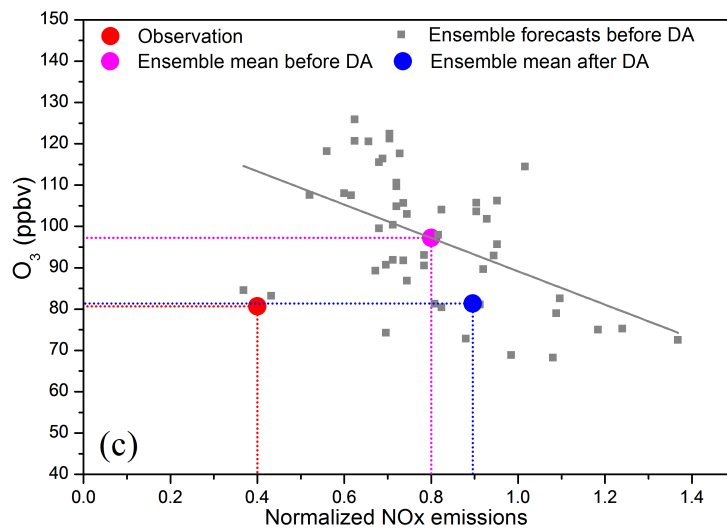


10





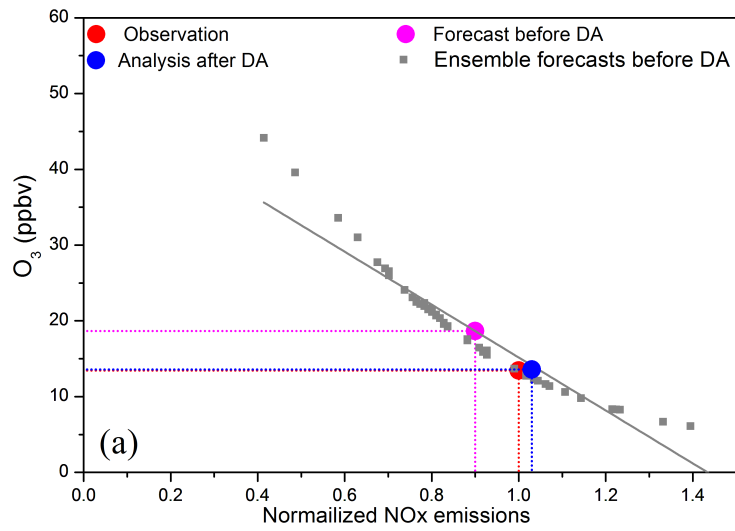
1



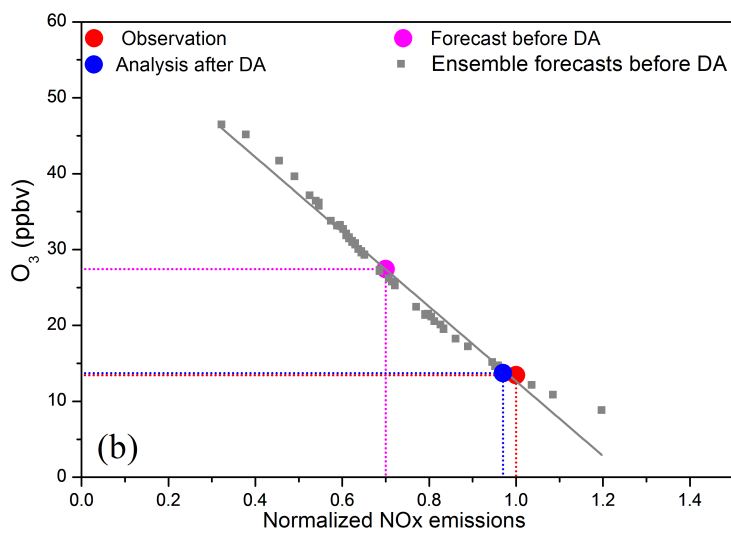
2

3 Figure 6 (a-c) O<sub>3</sub> concentrations (ppbv) and NO<sub>x</sub> emissions (no unit, normalized by the true NO<sub>x</sub>  
 4 emission) before and after data assimilation (DA) and their ensemble samples before DA at 12:00 LT  
 5 on August 12, 2008 in the three ideal DA experiments. The NO<sub>2</sub> photolysis rate is assumed to be  
 6 overestimated by 20%. (a) The prior NO<sub>x</sub> emission is overestimated by 30% and adjusted by the DA,  
 7 but the uncertainty of the NO<sub>2</sub> photolysis rate is missed (without perturbations on the NO<sub>2</sub> photolysis  
 8 rate) in the DA. (b) The same as the DA experiment in (a), but the uncertainty of the NO<sub>2</sub> photolysis  
 9 rate is taken into account through perturbing it. (c) The same as the DA experiment in (b), but the  
 10 bias in the prior NO<sub>x</sub> emission is increased to 100%. The magenta dot, the gray squares, the gray line,  
 11 the red dot and the blue dot represent the same as in Fig. 4.

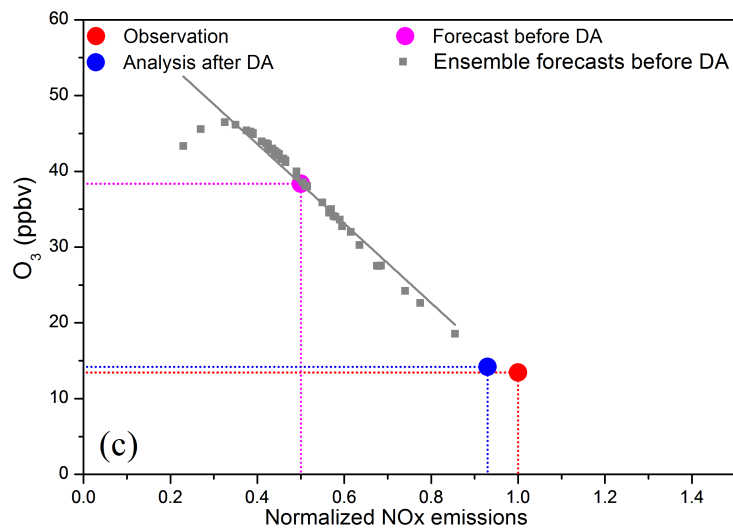
12



1



2



3

4 **Figure 7 (a-c)** O<sub>3</sub> concentrations (ppbv) and NO<sub>x</sub> emissions (no unit, normalized by the true NO<sub>x</sub>  
 5 emission) before and after data assimilation (DA) and their ensemble samples before DA 08:00 LT  
 6 on August 12, 2008 in the three ideal ozone data assimilation experiments with the prior NO<sub>x</sub>  
 7 emissions underestimated by 10% (a), 30% (b) and 50% (c) respectively. The magenta dot, the gray  
 8 squares, the gray line, the red dot and the blue dot represent the same information as Figs. 4.